09

Mode composition of waveguides based on hyperbolic van der Waals crystal in the visible range

© O.G. Matveeva[1], K.V. Voronin[2], D.V. Grudinin[1,3], S.D. Chikalkin[1,4], N.V. Pak[1], M.I. Titova[5], D.G. Baranov[1], A.A. Vishnevyy[1], V.S. Volkov[3], A.V. Arsenin[1,3]

[1] Center for Photonics and 2D Materials, Moscow Institute of Physics and Technology, Dolgoprudny, Russia
[2] Donostia International Physics Center (DIPC), Donostia/San-Sebastián, Spain
[3] Emerging Technologies Research Center, XPANCEO, Internet City, Dubai, United Arab Emirates
[4] Russian Quantum Center, Moscow, Russia
[5] Programmable Functional Materials Laboratory, Center for Neurophysics and Neuromorphic Technologies, Moscow, Russia
E-mail: matveeva@phystech.edu

Received June 17, 2025
Revised October 15, 2025
Accepted October 15, 2025

Optical waveguides are fundamental elements for nanotechnology applications due to their ability to efficiently transmit light signals at nanoscale. Plasmon polariton waveguides based on $MoOCl_2$, a hyperbolic van der Waals material with near-infrared and visible light performance, are demonstrated. A figure of merit (FOM) of approximately 40 is observed in the 530−960 nm range. Furthermore, a high degree of waveguide mode localization, up to $q = 15$, is observed. The dependence of the waveguide characteristics on the angle between the main waveguide axis and the in-plane crystallographic axes is also calculated.

Keywords: optical waveguides, hyperbolic plasmon polaritons, biaxial van der Waals crystal, superlocalized modes.

DOI: 10.61011/TPL.2026.02.63043.20409

In recent years, polaritons, which are hybrid states of light and matter arising when photons bind to quantum excitations of crystals (e.g., optical phonons or plasmons), have become a key tool for light control at subwavelength scales. Polariton modes are fundamental for such applications as plasmonic photocatalysis [1,2] and sensors [3], giant Raman scattering spectroscopy [4], wavefront control [5–7], and nonlinear optics [8,9].

The higher the effective refraction index of a polariton mode is, the stronger is the field localization in it (i.e., the smaller is the spatial scale of localization). The effective refraction index of a propagating wave in dielectrics (anisotropic ones included) is limited fundamentally by the largest component of the refraction index tensor. In contrast, if one or two principal values of permittivity in an anisotropic crystal are negative and the other values are positive, it may support waves with an arbitrarily high effective refraction index. A material of this kind is called hyperbolic, since isofrequency surfaces in the space of wave vectors form a hyperboloid; the electromagnetic waves supported by it are hyperbolic polaritons. Owing to their high effective refraction index, hyperbolic polaritons allow for localization of light on extremely subwavelength scales [10,11]. Hyperbolic materials, especially natural ones [12], are convenient for fabricating photonic elements, such as resonators [13], photonic crystals [14], and waveguides [15].

The study of geometric and chemical structure of crystals [16] provides an opportunity to find new materials for photonic applications. The $MoOCl_2$ van der Waals hyperbolic material [17–19] is unique in that it remains hyperbolic within a broad spectral band extending from the visible range to the near infrared one, whereas virtually all its known counterparts are hyperbolic in narrow intervals of the mid-infrared range.

In the present study, hyperbolic waveguides based on thin $MoOCl_2$ crystal films are examined numerically. The degree of mode localization and the range of their propagation are investigated, and the optimum waveguide parameters needed to maximize the propagation range are identified. Unlike dielectric waveguides of a similar size, which support one or two waveguide modes, a hyperbolic waveguide supports a technically infinite number of them (with the mode propagation length decreasing as the mode order increases) [20]. A classification of waveguide modes is given, and their evolution with a varying angle of wave propagation in an anisotropic film is revealed. In conclusion, the obtained results are compared with the properties of metal plasmonic waveguides. The waveguides examined here support superlocalized modes with low propagation losses, which opens up new opportunities in high-frequency two-dimensional optoelectronics.

It can be seen in Fig. 1 that the waveguide was modeled so that the [100] component of the dielectric tensor was coaxial with the principal axis of the waveguide (Fig. 1, *a*), since a hyperbolic law of wave propagation with the wave propagating either along the [100] direction or at a certain acute angle to it is seen within the wavelength range of 530−960 nm. This is attributable to the fact that $\mathrm{Re}\varepsilon_{100} < 0$ and $\mathrm{Re}\varepsilon_{001} > 0$ within this frequency range (Fig. 1, *b*), which, in turn, is due to the chemical composition and

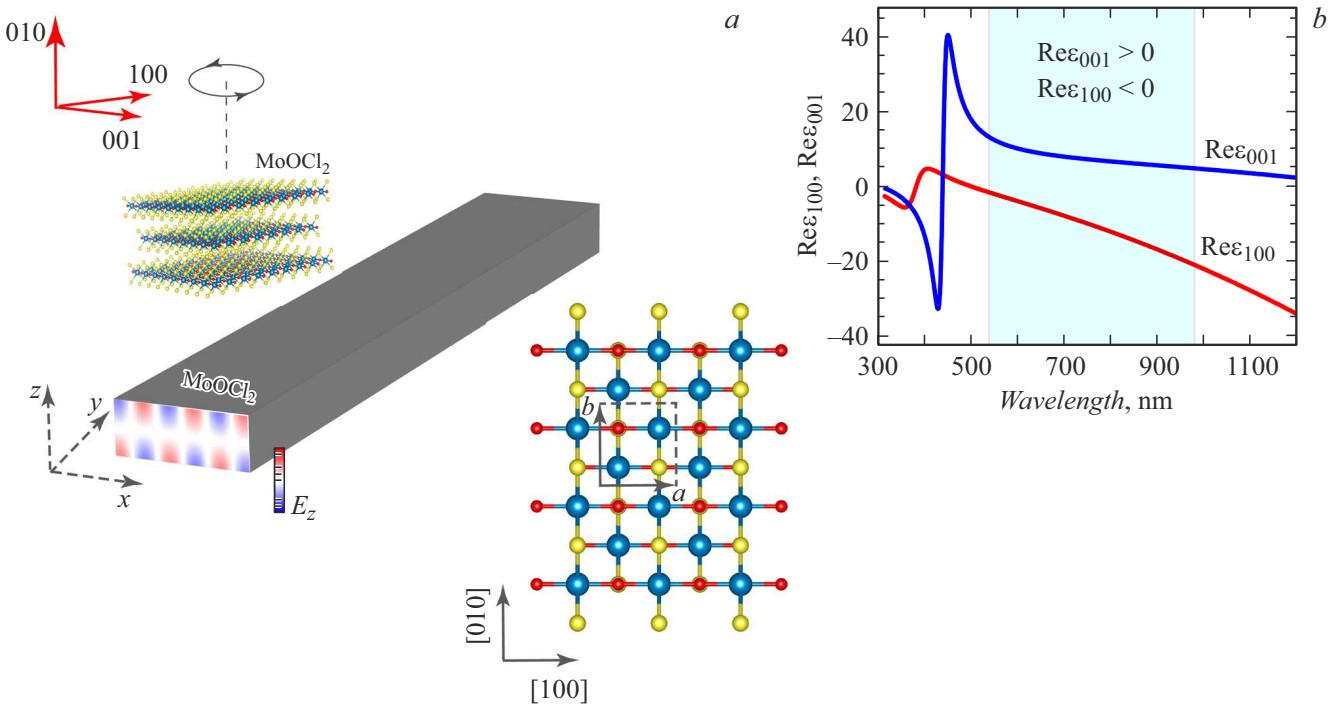

Figure 1. Plasmon polariton waveguides in $MoOCl_2$. *a* — Diagrams illustrating the possibility of orienting a waveguide at an arbitrary angle to the optical crystal axes and the crystal lattice structure (molybdenum nuclei are shown in blue; oxygen nuclei, in red; chlorine nuclei, in yellow) with a unit cell (a, b) of the $MoOCl_2$ material. *b* — Dependence of the in-plane dielectric functions on the wavelength of incident light; the region of hyperbolic behavior of the material is marked in blue. A color version of the figure is provided in the online version of the paper.

geometric properties of the crystal lattice. The width and height of our waveguide are 100 and 50 nm, respectively.

Examining the modes arising in the waveguide, we classified them according to the number of oscillations of the y-electric field component in the vertical and horizontal directions in the waveguide cross section (Fig. 2, *a*). When the $q(\lambda)$ dispersion (wave number $q = \frac{|\mathbf{k}|}{k_0}$, $k_0 = \frac{2\pi}{\lambda}$, and $\mathbf{k}$ is the wave vector) was plotted, it was noted that a new family of dispersion curves M_{1i}, which intersect the dispersion curves from zero family M_{0i} and originate from mode M_{10}, emerges (Fig. 2, *b*). Having examined the intersection points in more detail, we found that they have the same real part of wave number Req, but different imaginary parts Imq, which is attributed to an increase in losses with an increase in number of oscillations i in the horizontal direction in the waveguide cross section. This raises the issue of Q factor of different modes.

To evaluate the quality characteristics of different modes, we calculate their path length in the waveguide (Fig. 3, *b*)

$$L_{decay} = \frac{1}{\mathrm{Im}k}. \qquad (1)$$

In addition, we calculate the ratio of real and imaginary parts of the wave vector modulus (figure of merit, FOM; see Fig. 3, *a*), which is proportional to the ratio of mean free path L_{decay} of a polariton to its wavelength λ_{pol}, for each mode:

$$\mathrm{FOM} = \frac{\mathrm{Re}k}{\mathrm{Im}k} = 2\pi\frac{L_{decay}}{\lambda_{pol}}. \qquad (2)$$

The dependences presented in Fig. 3 suggest an unexpected conclusion that the Q factor of the more localized first mode (M_{10}) is higher than that of fundamental mode M_{00}, which, however, propagates further. Thus, the $MoOCl_2$ material is suitable for information applications of photonics, since it addresses their primary challenge: fit as much information as possible into a minimum space with minimal losses in signal propagation.

The in-plane anisotropy of the material provides an additional degree of freedom to the object under study, which allows one to draw a conclusion regarding the nature of influence of the angle between the principal waveguide axis and the direction of wave propagation in the crystal corresponding to the shortest possible wave vector (along the [100] crystal axis) on the degree of localization of modes in the waveguide. Comparing modes M_{04} and M_{10} (see the inset in Fig. 4, *a*), one finds that the degree of localization of both modes decreases with increasing angle (Figs. 4, *a*, *b*, scale on the left, solid curves), which is contradictory to what is observed in the film. The Q factor of modes also decreases (Figs. 4, *a*, *b*, scale on the right, dashed curves). The observed dependence will remain valid with a further increase in angle due to the monotonicity of the function

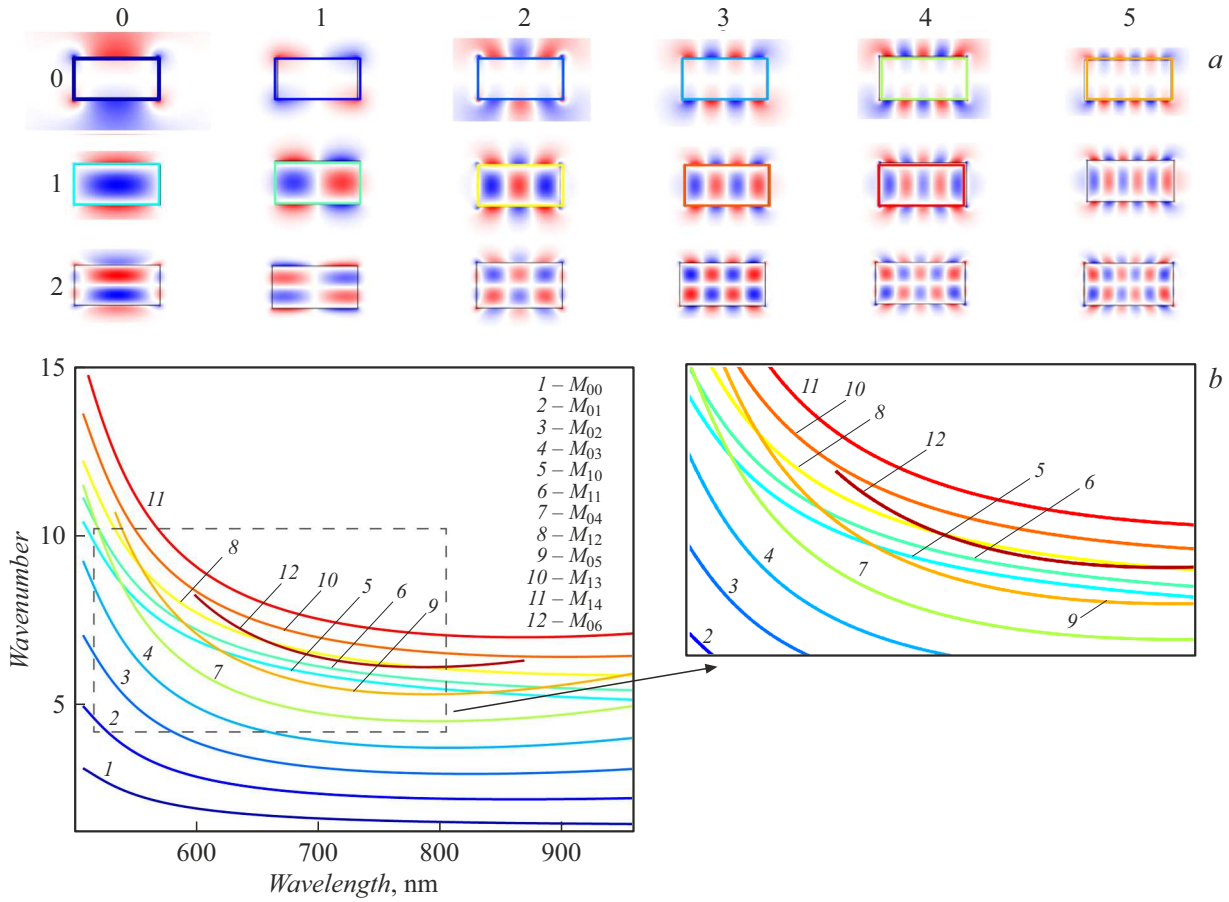

Figure 2. Classification of waveguide modes. *a* — Distribution of the real part of the vertical component of electric field E_y for modes M_{ij} (i — row, j — column) of a waveguide with a cross section of 100 × 50 nm at a wavelength of 570 nm (a color version of the figure is provided in the online version of the paper). *b* — Dispersion of waveguide modes in a waveguide with a cross section of 100 × 50 nm.

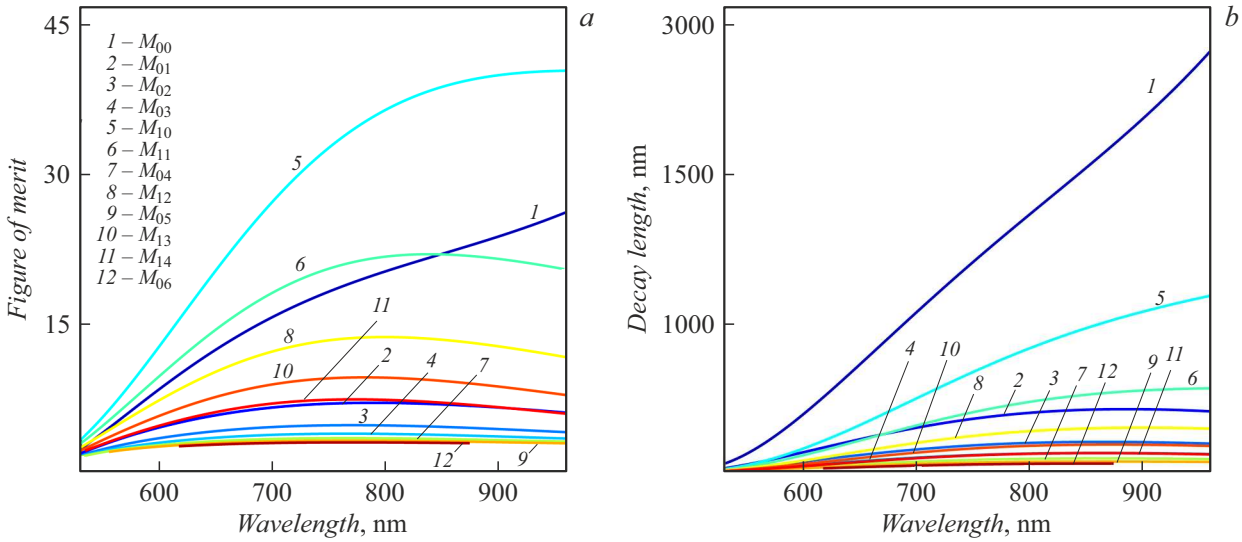

Figure 3. Qualitative characteristics of waveguide modes. *a* — FOM of waveguide modes in a waveguide with a cross section of 100 × 50 nm oriented along the [100] axis. *b* — Wavelength dependences of the decay length for different modes.

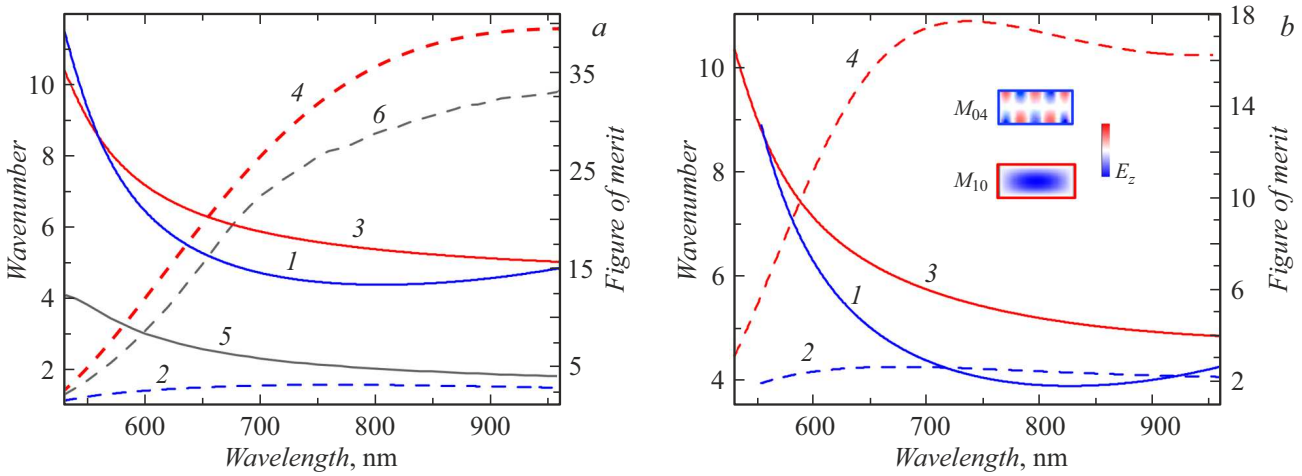

Figure 4. Comparative characteristics of modes M_{04} (*1*, *2*) and M_{10} (*3*, *4*) for waveguides oriented along the [100] axis and at an angle of 5° to it, as well as the symmetric mode in metal (*5*, *6*). *a* — Dispersions of modes M_{04} and M_{10} for an angle of 0°, as well as the metallic mode (solid curves; scale on the left); FOM of modes M_{04} and M_{10} for an angle of 0°, as well as the metallic mode (dashed curves; scale on the right). *b* — Dispersions of modes M_{04} and M_{10} for an angle of 5° (solid curves; scale on the left); FOM of modes M_{04} and M_{10} for an angle of 5° (dashed curves; scale on the right).

defining the wave number with respect to the angle of wave propagation. This observation allows us to conclude that it makes sense in actual applications to fabricate waveguides coaxially with [100] in the hyperbolic crystal in question.

In conclusion, we note that an ultrahigh degree of localization of waveguide modes (up to $q = 15$, which is significantly higher than in metal waveguides of a similar size) was observed in the present study. To put this into perspective, the localization in a rectangular gold waveguide with a cross section of 100×50 nm is just $q = 4$. The Q factor of the M_{10} mode exceeds that of the mode in a gold waveguide (Fig. 4, *a*, curves *5* and *6*).

Thus, the mode structure of a waveguide based on a hyperbolic material was presented. It differs qualitatively from the one of a conventional dielectric waveguide in the presence of increasingly higher degrees of localization at higher mode orders. In addition, it was found that higher modes are not only more localized, but also have a higher Q factor than lower-order modes. This is bound to facilitate the use of $MoOCl_2$ in fabrication of high-grade optical waveguides.

Funding

This study was supported by the Russian Science Foundation (grant 24-79-00308).

Conflict of interest

The authors declare that they have no conflict of interest.

References

[1] E. Cortés, L.V. Besteiro, A. Alabastri, A. Baldi, G. Tagliabue, A. Demetriadou, P. Narang, ACS Nano, **14**, 16202 (2020). DOI: 10.1021/acsnano.0c08773

[2] M. Herran, S. Juergensen, M. Kessens, D. Hoeing, A. Köppen, A. Sousa-Castillo, W.J. Parak, H. Lange, S. Reich, F. Schulz, E. Cortés, Nat. Catal., **6**, 1205 (2023). DOI: 10.1038/s41929-023-01053-9

[3] Y. Xu, P. Bai, X. Zhou, Yu. Akimov, C.E. Png, L.-K. Ang, W. Knoll, L. Wu, Adv. Opt. Mater., **7**, 1801433 (2019). DOI: 10.1002/adom.201801433

[4] J. Langer, D. Jimenez de Aberasturi, J. Aizpurua, R.A. Alvarez-Puebla, B. Auguié, J.J. Baumberg, G.C. Bazan, S.E.J. Bell, A. Boisen, A.G. Brolo, J. Choo, D. Cialla-May, V. Deckert, L. Fabris, K. Faulds, F.J. García de Abajo, R. Goodacre, D. Graham, A.J. Haes, C.L. Haynes, C. Huck, T. Itoh, M. Kall, J. Kneipp, N.A. Kotov, H. Kuang, E.C. Le Ru, H.K. Lee, J.-F. Li, X.Y. Ling, S.A. Maier, T. Mayerhöfer, M. Moskovits, K. Murakoshi, J.-M. Nam, S. Nie, Y. Ozaki, I. Pastoriza-Santos, J. Perez-Juste, J. Popp, A. Pucci, S. Reich, B. Ren, G.C. Schatz, T. Shegai, S. Schlücker, L.-L. Tay, K.G. Thomas, Z.-Q. Tian, R.P. Van Duyne, T. Vo-Dinh, Y. Wang, K.A. Willets, C. Xu, H. Xu, Y. Xu, Y.S. Yamamoto, B. Zhao, L.M. Liz-Marzań, ACS Nano, **14**, 28 (2020). DOI: 10.1021/acsnano.9b04224

[5] N. Yu, P. Genevet, M.A. Kats, F. Aieta, J.-P. Tetienne, F. Capasso, Z. Gaburro, Science, **334**, 333 (2011). DOI: 10.1126/science.1210713

[6] P. Genevet, D. Wintz, A. Ambrosio, A. She, R. Blanchard, F. Capasso, Nat. Nanotechnol., **10**, 804 (2015). DOI: 10.1038/nnano.2015.137

[7] D. Wintz, A. Ambrosio, A.Y. Zhu, P. Genevet, F. Capasso, ACS Photon., **4**, 22 (2017). DOI: 10.1021/acsphotonics.6b00758

[8] J. Lee, M. Tymchenko, C. Argyropoulos, P.-Y. Chen, F. Lu, F. Demmerle, G. Boehm, M.-C. Amann, A. Alú, M.A. Belkin, Nature, **511**, 65 (2014). DOI: 10.1038/nature13455
[9] M. Mesch, B. Metzger, M. Hentschel, H. Giessen, Nano Lett., **16**, 3155 (2016). DOI: 10.1103/PhysRevLett.117.123904
[10] E. Galiffi, G. Carini, X. Ni, G. Álvarez-Pérez, S. Yves, E.M. Renzi, R. Nolen, S. Wasserroth, M. Wolf, P. Alonso-Gonzalez, A. Paarmann, A. Alú, Nat. Rev. Mater., **9**, 9 (2023). DOI: 10.1038/s41578-023-00620-7
[11] M. Tamagnone, A. Ambrosio, K. Chaudhary, L.A. Jauregui, P. Kim, W.L. Wilson, F. Capasso, Sci. Adv., **4**, eaat7189 (2018). DOI: 10.1126/sciadv.aat7189
[12] W. Ma, P. Alonso-González, S. Li, A.Y Nikitin, J. Yuan, J. Martín-Sánchez, J. Taboada-Gutiérrez, I. Amenabar, P. Li, S. Vélez, C. Tollan, Z. Dai, Y. Zhang, S. Sriram, K. Kalantar-Zadeh, S.-T. Lee, R. Hillenbrand, Q. Bao, Nature, **562**, 557 (2018). DOI: 10.1038/s41586-018-0618-9
[13] O.G. Matveeva, A.I.F. Tresguerres-Mata, R.V. Kirtaev, K.V. Voronin, J. Taboada-Gutiérrez, C. Lanza, J. Duan, J. Martín-Sánchez, V.S. Volkov, P. Alonso-González, A.Y. Nikitin, npj 2D Mater. Appl., **7**, 31 (2023). DOI: 10.1038/s41699-023-00387-z
[14] N. Capote-Robayna, O.G. Matveeva, V.S. Volkov, P. Alonso-Gonzalez, A.Y. Nikitin, Laser Photon. Rev., **16**, 9 (2022). DOI: 10.1002/lpor.202200428
[15] D. Grudinin, O. Matveeva, G. Ermolaev, A. Vyshnevyy, A. Arsenin, V. Volkov, Photonics, **10**, 59 (2023). DOI: 10.3390/photonics10010059
[16] A.S. Slavich, G.A. Ermolaev, M.K. Tatmyshevskiy, A.N. Toksumakov, O.G. Matveeva, D.V. Grudinin, K.V. Voronin, A. Mazitov, K.V. Kravtsov, A.V. Syuy, D.M. Tsymbarenko, M.S. Mironov, S.M. Novikov, I. Kruglov, D.A. Ghazaryan, A.A. Vyshnevyy, A.V. Arsenin, V.S. Volkov, K.S. Novoselov, Light Sci. Appl., **13**, 68 (2024). DOI: 10.1038/s41377-024-01407-3
[17] Z. Wang, M. Huang, J. Zhao, C. Chen, H. Huang, X. Wang, P. Liu, J. Wang, J. Xiang, C. Feng, Z. Zhang, X. Cui, Y. Lu, S.A. Yang, B. Xiang, Phys. Rev. Mater., **4**, 041001(R) (2020). DOI: 10.1103/PhysRevMaterials.4.041001
[18] G. Venturi, A. Mancini, N. Melchioni, S. Chiodini, A. Ambrosio, Nat. Commun., **15**, 9727 (2024). DOI: 10.1038/s41467-024-53988-7
[19] F.L. Ruta, Y. Shao, S. Acharya, A. Mu, N.H. Jo, S.H. Ryu, D. Balatsky, Y. Su, D. Pashov, B.S.Y. Kim, M.I. Katsnelson, J.G. Analytis, E. Rotenberg, A.J. Millis, M. van Schilfgaarde, D.N. Basov, Science, **387**, 786791 (2025). DOI: 10.1126/science.adr5926
[20] G. Álvarez-Pérez, K.V. Voronin, V.S. Volkov, P. Alonso-González, A.Y. Nikitin, Phys. Rev. B, **100**, 11 (2019). DOI: 10.1103/PhysRevB.100.235408

Translated by D.Safin